S-wave Splitting in Central Apennines (Italy): anisotropic parameters in the crust during seismic sequences

Article *in* Annals of geophysics = Annali di geofisica · May 2023

DOI: 10.4401/ag-8844

CITATIONS
2

READS
98

4 authors:

Marina Pastori
National Institute of Geophysics and Volcanology
43 PUBLICATIONS **694** CITATIONS
SEE PROFILE

Paola Baccheschi
National Institute of Geophysics and Volcanology
51 PUBLICATIONS **328** CITATIONS
SEE PROFILE

Davide Piccinini
National Institute of Geophysics and Volcanology
144 PUBLICATIONS **3,477** CITATIONS
SEE PROFILE

Lucia Margheriti
National Institute of Geophysics and Volcanology
214 PUBLICATIONS **4,198** CITATIONS
SEE PROFILE

ANNALS OF GEOPHYSICS, 66, 2023; doi: 10.4401/ag-8844
OPEN ACCESS

S-wave Splitting in Central Apennines (Italy): anisotropic parameters in the crust during seismic sequences

Marina Pastori[*,1], Paola Baccheschi[1], Davide Piccinini[2] and Lucia Margheriti[1]

(1) Istituto Nazionale di Geofisica e Vulcanologia, Osservatorio Nazionale Terremoti, Via di Vigna Murata 605, 00143, Roma, Italy
(2) Istituto Nazionale di Geofisica e Vulcanologia, Sezione Di Pisa, Via Cesare Battisti 53, 56125, Pisa, Italy

Article history: received May 13, 2022; accepted November 9, 2022

Abstract

In this work, we reviewed the main anisotropic results obtained in the last two decades along the Central Apennines. Moreover, we improved this database, with new results coming from the seismicity that occurred in the Montereale area, between 2009 and 2017, which corresponds to a spatio-temporal gap in the previously analyzed datasets.
The examined papers concerned both seismic sequences (as Colfiorito in 1997, Pietralunga in 2010, L'Aquila in 2009, Amatrice in 2016) and background seismicity (as the 2000-2001 Città di Castello experiment).
The whole of the collected results shows a general NW-SE fast shear wave direction consistent with both the orientation of the extensional active Quaternary and inherited compressive fault systems, focal mechanisms and local stress field. Also, we observed a more intense anisotropy strength (normalized delay time >0.006 s/km) nearby the strongest events ($M>5$), all concentrated in the hanging-wall of the activated fault systems. In fact, this area is deeply affected by the surrounding rock volume perturbations that, in turn, have altered both the local stress field and crustal fracturing network.
The most common anisotropic interpretative models that could explain our results are 1) the stress-induced anisotropy according to the Extensive-Dilatancy Anisotropy (EDA) model where the anisotropic pattern is related to the local stress variation and most of the variability is visible in time; 2) the tectonic-controlled anisotropy according to the Structural-Induced Anisotropy (SIA) model where the anisotropic pattern is related to the major structural features and most of the variability is visible only in space.
As reported by the examined studies in Central Apennines the possibility to discriminate between stress and structural anisotropy is quite complex in a region where the directions of the extensional regime, the in situ horizontal maximum stress, the strike of major faults, both active and inherited coincide. Generally, in this review, we noted an overlap and mixture of the two aforementioned mechanisms and, just through a temporal analysis, made in the Montereale area, we supposed a predominant stress-induced anisotropy only in rock volumes where anisotropic parameter variations have been detected.

Keywords: Shear wave splitting; Crustal seismic anisotropy; Seismic sequences; Central Apennines; Fluids in the crust

1. Introduction

Central Apennines is a region of high seismic hazards. In fact, in the last decades it was affected by several moderate to strong mainshocks (Figure 1) followed by seismic sequences of thousands of aftershocks. Here, we mention the three major ones: M_w 6.0 Umbria-Marche 1997 [Amato et al. 1998], M_w 6.3 L'Aquila 2009 [Chiarabba et al., 2009], M_w 6.5 Amatrice-Visso-Norcia 2016-2017 [Improta et al., 2019].

The Central Apennines Mountain chain is a fold-and-thrust belt characterized by present-day NE-SW extensional tectonics and NW-SE-trending active normal faults, mostly parallel to the dominant horizontal maximum stress [Mariucci and Montone, 2016]. The higher deformation rates are found along the axis of the mountain chain [D'Agostino et al., 2011] where most of the seismicity and historical strong earthquakes also occur. To monitor this area, several permanent seismic stations have been installed and during the seismic crises, other ones temporary are deployed. The union between the stations' coverage and the occurrence of the earthquakes allow us to have a lot of data to investigate shear wave splitting in this area. The region is also affected by widespread CO_2 degassing occurrences and deep fluid circulation [Chiodini et al., 2020], which could facilitate fault reactivation and thus reduce the recurrence time of an earthquake. The anomalous flux of CO_2 suddenly disappears in the Central Apennines in correspondence to a narrowband where most of the seismicity concentrates. Here, at depth, the gas accumulates in crustal traps, generating over pressurized CO_2 reservoirs which induce seismicity. The circulation and the state of fluids at depth could facilitate fault reactivation, reducing the recurrence time of a moderate to large earthquake.

In areas where active faults are present, stress field variation controls fracture field orientation and fluid migration processes and the state of the fluid in the rock, whose evolution with time can be observed through the monitoring of anisotropic parameters, possibly providing useful information about the fault failure process.

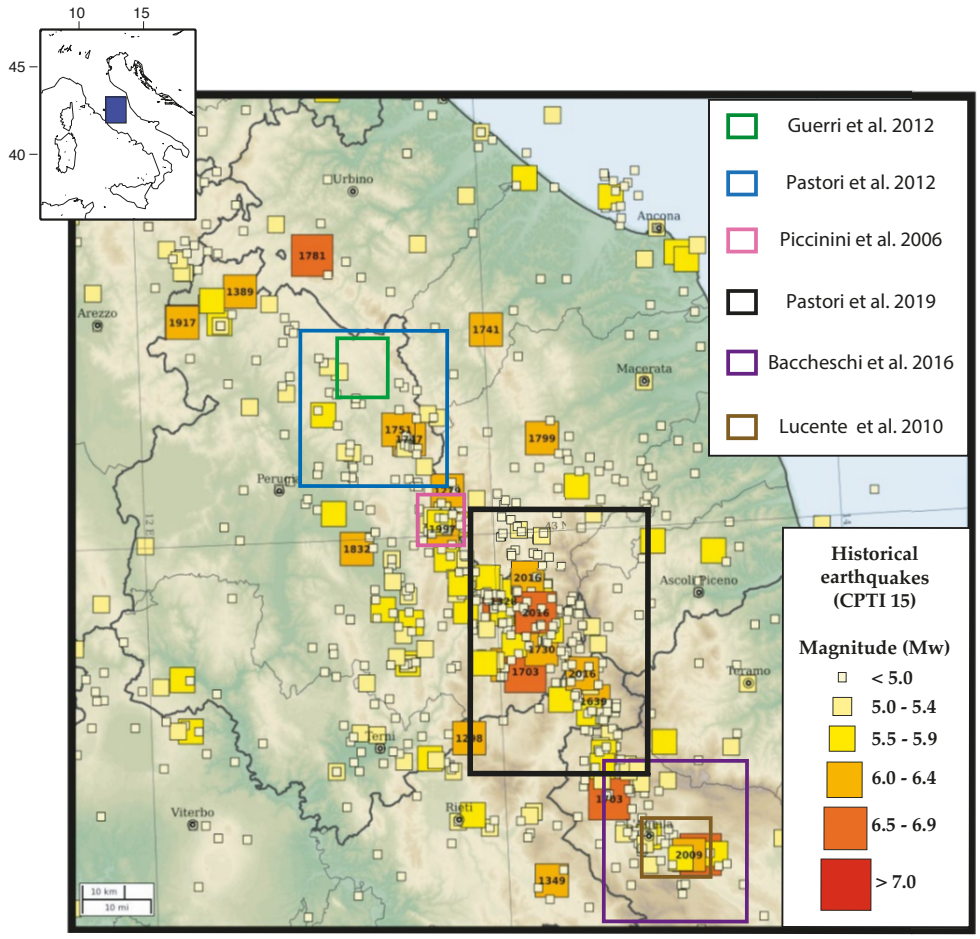

Figure 1. Map of large earthquakes in the central Apennines according to the "Catalogo Parametrico dei Terremoti Italiani" CPTI15 [CPTI15, Rovida et al., 2022; https://doi.org/10.13127/CPTI/CPTI15.4]. The color boxes are the region studied in the six papers about seismic anisotropy in the crust of Central Italy.

In the last decades, the central Apennines has been the object of several studies (Figure 1) aimed to retrieve the anisotropic parameters of the crust. They all produced high-quality anisotropic results, and we reported individual measurements in a unique single Excel file (Table A1) in the appendix section.

Some studies analyzed the background seismicity or minor earthquake sequences [Pastori et al., 2012; Guerri et al., 2012], while others, in the southern portion of the investigated region, analyzed the seismic sequences associated with mainshock having magnitude Mw equal or greater than 6.0 [Piccinini et al., 2006; Lucente et al., 2010; Baccheschi et al., 2016; Pastori et al., 2019].

In these papers we tried to distinguish the prevailing contribution between crustal sources of anisotropy, moreover, we implemented the anisotropic database, coming from the six cited papers (Figure 1), by analyzing, in this new work, the seismicity recorded at 3 sites (RM10/RM33 at a common site, as well as, CAMP and, SMA1) between 2009 and 2017 in the Montereale area, which corresponds to a spatio-temporal gap between the north termination of the L'Aquila sequence and the south of the Amatrice one. The whole of the collected results is discussed, considering the active stress and the fracturing field in Central Apennines to define the most likely cause of seismic anisotropy in the crust and how it relates to the seismogenic process.

1.1 Shear wave splitting in the crust

The most common phenomenon that testifies to the anisotropic properties of the crust is *Shear Wave Splitting* (*SWS*). When a shear wave passes through an anisotropic medium on its path to the receiver, it splits into two components, called fast and slow components, which travel at different speeds and are polarized normal to each other [Vinnik and Kind,1993; Savage, 1999; Bowman and Ando, 1987]. Two splitting parameters are used to describe an anisotropic medium: the polarization azimuth of the fast shear wave, φ, which defines the preferred orientation of the anisotropic crystals; and the delay time, δt, between the fast and slow wave arrivals, which is a measure of the thickness and of the strength of the anisotropic layer.

Sometimes, it can happen that a shear wave does not show splitting, in this case, we are observing a null measurement, and it is identified by a delay time value proximate to zero. The S-wave splitting may not occur for two reasons: (1) the presence of an isotropic media and (2) the S-wave travels with the initial polarization parallel to the fast or slow directions of the anisotropic media [Schutt et al., 1998]. In this second case, even if we cannot observe the splitting of the shear wave, we can use the results since they identify the direction of one of the anisotropy axes. In the shallow crust, two main mechanisms are responsible for the observed shear-wave anisotropy: 1) the stress-induced anisotropy, also known as Extensive-Dilatancy Anisotropy (EDA) model, given by the alignment of vertical, fluid-filled microcracks favorably oriented by the regional compressive stress so that the fast directions are oriented parallel to the horizontal maximum stress (S_{Hmax}) direction [Boness and Zoback, 2006; Gao et al., 1998, 2011; Gao and Crampin, 2008; Martin et al., 2014]; 2) the structure-induced anisotropy (SIA), arising from the preferential alignment of macroscopic structural features such as finely-layered sedimentary sequences, pervasive fault-zone fabric, macroscopic aligned fractures, and preferentially oriented anisotropic minerals giving rise to the foliation in metamorphic rocks [Zinke and Zoback 2000; Verdon et al., 2008].

Several SWS measurements worldwide have shown a sharp coherence between φ and S_{Hmax}, promoting the EDA-cracks as the primary cause of shear wave splitting in the crust [Gao and Crampin, 2008 and references therein]. Stress-induced anisotropy has been suggested to explain the pattern of seismic anisotropy in central Japan [Hiramatsu et al., 2010] and in the fore-arc of the Northern Cascadia subduction zone [Balfour et al., 2012]. On the other hand, structural-controlled anisotropy has been proposed for the Karadere-Düzce branch of the North Anatolian Fault [Li et al. 2014], for the Eastern Betic Cordillera, Spain [Buontempo et al., 2013], around the Gulf of Corinth, Greece [Kapetanidis et al., 2021; Bouin et al., 1996], the Atotsugawa Fault, Japan [Mizuno et al. 2005] and in Northern Cascadia [Matharu et al., 2014].

The anisotropic properties within the fault zone and the surrounding rock volume might often result from the mixture of both structural and stress-induced mechanisms. This circumstance makes it quite difficult to discriminate which of the two mechanisms is responsible for the observed anisotropy. What is commonly noted is the overlap of the two mechanisms, with stress-aligned microcracks away from the fault and shear fabric-controlled anisotropy close to the damage zone: this has been observed around the San Andreas Fault [Zhang and Schwartz, 1994; Boness and Zoback, 2004, 2006; Cochran et al., 2006]; near Parkfield, California, [Liu et al., 1997, 2008], in Northwest Turkey, [Hurd and Bohnhoff 2012; Eken et al., 2013]; around the Greendale Fault, New

Zealand [Syracuse et al. 2012]. In the extensional regimes, the S_{Hmax} direction coincides with the strike of the main active faults, so that, the contribution from structural-related anisotropy cannot be completely ruled out because of the sharp coherence between the leading polarization direction and the dominant strike of active faults in the region. This is the case of the axial zone of the Italian Peninsula currently underwent to extensional tectonics and where the crustal anisotropy has been explained by a mixture of stress and structural induced anisotropy [i.e Baccheschi et al., 2016; Pastori et al., 2019].

Stress-aligned shear wave splitting is highly sensitive to stress field changes. Fault growth processes due to the coseismic slip accumulation and the change in the local stress field are interdependent phenomena and cause a re-orientation of microcracks and, thus, of fast axes. Such evidence highlights the relationship that occurs between coseismic changes in anisotropic parameters and stress changes before and after an earthquake. In addition, the observed pattern of anisotropy could be associated with the presence of a fluid-rich zone associated with a heavily fractured and overpressurized rock volume within the damage fault zone. In this case, it is likely that the damage zone underwent different physical conditions with respect to the surrounding crustal volume. This results in a reorganizing of microcracks geometry, and consequently of fast axes directions, at different angles with respect to the S_{Hmax} direction [Padhy and Crampin, 2006].

The main causes of fracture preferential alignment are: 1) past tectonic phases that may not be related to the currently active stress in a region [Zinke and Zoback, 2000]; 2) the ongoing formation and alignment of fluid-filled micro-cracks due to the active stress field [EDA model, Crampin 1991]. In this second case, time-variations of the stress field might alter the pore pressure [Zatsepin and Crampin, 1997], which is considered in the anisotropic poro-elasticity (APE) model.

2. Data and methods

The possibility to discriminate between stress and structural anisotropy is quite complex in an extensional regime due to the coincidence of the S_{Hmax} direction and the strike of major faults, as reported by several studies in Central Apennines above-mentioned.

Our experience leads us to believe that the anisotropic pattern is mainly related to a local stress variation, according to the EDA-APE model, where most of the variability is visible in time, otherwise, it will be related to a structural-induced anisotropy (SIA model) where the pattern variability is visible only in space.

In this review, the Amatrice [Pastori et al., 2019] and L'Aquila [Baccheschi et al., 2016] high-quality splitting datasets were reworked along with an additional dataset, in order to fill the temporal gap 2011-2015 in the overlap area between these two sequences. This area corresponds to the north termination for the L'Aquila sequence and south for the Amatrice one, where the Montereale seismic source produced a $M = 5.2$ and $M = 5.5$, respectively.

With the purpose of better understanding the anisotropic variations, in space and in time, and distinguishing the prevailing contribution between crustal sources of anisotropy of this area, we collected data recorded by four stations belonging to INGV permanent seismic network IV (RM10; RM33; SMA1; CAMP), continuously working in the overlap area in the period 2009-2017 (further details are listed in Table 1).

Station Name	Start	Stop	Number of events
CAMP	01/01/2009	31/12/2017	7694
RM10	07/04/2009	08/12/2009	2628
RM33	08/09/2010	31/12/2017	6922
SMA1	13/08/2009	31/12/2017	8126

Table 1. List of used stations and relative downloaded events in their working period.

From here on out, RM10 and RM33 stations are considered as a single site because they are located in the nearby position and worked in temporal continuity: in 2009 and from 2010 up to now (with an interruption between 2012 and 2013), respectively.

Three-component waveforms, sampled at 125 sps, were downloaded using OBSPY code (https://docs.obspy.org/index.html), by directly accessing the SeisComP Data Structure (SDS) structure of the INGV waveform archive.

To avoid that source complexity may introduce a bias in shear wave splitting evaluations, we keep only earthquake waveforms with $M < 4$ located at a maximum distance of 20 km from each station. To guarantee that the S waves do not interact with any free surface or horizontal interface and to avoid contamination by P to S converting phases, we selected only events within the shear-wave window [Crampin et al., 2001], that is, the cone of ray paths with angles of incidence to the free surface of less than 45° [Evans, 1984]. This criterion ensures that we are using only the real S-direct arrival phases at the station.

Origin time, P and S wave arrivals for the selected events were obtained by querying the INGV Web Service (http://terremoti.ingv.it/webservices_and_software). The total number of seismic events downloaded was 25370.

Splitting results are obtained using Anisomat + [Piccinini et al., 2013], a semi-automatic Matlab code to retrieve anisotropic parameters, φ and δt, from three-component seismograms, based on the cross-correlation matrix method [Bowman and Ando, 1987].

This allows the evaluation of the similarity of the pulse shape between the radial and transversal S-waves and their temporal lag. In fact, the S-wave horizontal components usually show similar forms with mutually perpendicular oscillation directions and different travelling velocities according to their propagation direction. To estimate anisotropic parameters, the cross-correlation coefficient is computed for each rotational step of 1° (from 0 to 180°) of the horizontal components. Then, by means of a grid search on the obtained two-dimensional matrix, the code evaluates the couple $\delta t - \varphi$ which maximizes the cross-correlation coefficient (XC). To obtain a sub-sample precision, we apply a common technique based on fitting of the five samples in the neighborhood of the peak correlation value by a second-order polynomial interpolation.

Associated δt and φ errors are defined by a criterion that reflects the shape of the cross-correlation matrix and how rapidly the matrix grows around the observed maximum value. In practice, the goodness of the estimation is related to the difference in delay time and in degrees between the cross-correlation maximum and 95% of the parameter values themselves.

We used a tuned and tested configuration to obtain the optimal estimation results for local earthquakes, also used to analyze the Amatrice and L'Aquila sequences, applying the following setting values: 1) cut-off frequencies $cf1 = 1$ and $cf2 = 12$ Hz of a bandpass fourth-order two-pass Butterworth filter; 2) S-to-P amplitude ratio ≥ 4; 3) amplitude sum of horizontal components greater than the amplitude of vertical component (H/V ratio > 1); 4) analysis window length of ~0.35 s, obtained by the relation

$$WL = PRE + DUR \tag{1}$$

where PRE is the parameter that identifies the start of the window, in this case, 0.15 s before the S-picking while DUR is the time after the S-picking obtained by the formula

$$DUR = C\frac{1}{cf2} \tag{2}$$

where C coefficient is 2.5 that ensure the involving of more than a whole cycle of the filter corner frequency.

After performing the splitting evaluation, we have further selected the results, that is, we considered as good a measurement having a cross-correlation value greater or equal to 0.75. Then we distinguished the measurements to "fast", when the delay time is greater than 0.02 s, or "null", for delay times less or equal to 0.02 s. Overall, with this new elaboration, we obtained 9610 fast and 9578 null measurements, starting from a raw dataset composed of 24859 event-station pairs. In Table 2 is reported a summary of the numbers of the analyzed event-station pairs and the resulting measurements differentiate for each dataset, which we will discuss in the next sections.

Dataset Name	Total event-station pairs	N° Fast measurements	N° Null measurements
L'Aquila (2009)	3624	1526	1413
Amatrice (2016-2017)	34453	11862	15322
Montereale (2009-2017)	24859	9610	9578

Table 2. Summary for each dataset of the analyzed event-station pairs and the resulting fast and null measurement numbers. The total number of the event-station pairs, indicated in column 2, includes all the downloaded data before any kind of quality selection.

3. New Results

In this section, we describe only the data coming from three sites, involving four stations, working in the overlap area in the period 2009-2017. In Figure 2, the structural setting and all the analyzed events are displayed and in Table 3 the φ, δt, δtn mean values and associated errors, evaluated at each station, are reported.

Site Name	N° measurements	$\overline{\varphi}$ (°)	$\overline{\varphi}$ error (°)	$\overline{\delta t}$ (s)	$\overline{\delta t}$ error (s)	$\overline{\delta tn}$ (s/km)	$\overline{\delta tn}$ error (s/km)
RM10/ RM33	3131 (115/3016)	N156 (N162/N155)	13.6 (14.5/13.6)	0.062 (0.056/0.062)	0.007 (0.008/0.007)	0.0043 (0.0053/0.0043)	0.00004 (0.00023/0.0004)
CAMP	4017	N128	12.5	0.058	0.012	0.0039	0.00003
SMA1	2462	N170	12.4	0.066	0.008	0.0044	0.00004
TOTAL	9610	N147	12.8	0.061	0.009	0.0041	0.00002

Table 3. Summary for each site of the resulting measurements, average values of φ, δt, δtn parameters and associated errors. For site RM10/RM33, values in parentheses refer to measurements at each station, the first value is for RM10 and the second is for RM33.

In order to better visualize the anisotropic pattern, we mapped the φ directions by means of the Tomography Estimation of Shear wave splitting and Spatial Averaging code [TESSA; Johnson et al., 2011]. We used a regular grid with boxes 2 km × 2 km wide, producing 126/1024 active boxes in which at least 10 rays pass through. The regular grid setting ensures the anchorage of the box center is always at the same position, in this way we can compare the results also over time. The black bars represent the obtained mean φ direction, which is displayed only if in each cell the standard deviation and the standard error of the mean are less than 30° and 10°, respectively. Furthermore, the data are also weighted according to the uncertainties on the individual φ measurements computed by Anisomat + and to the weighting regime selected; for this analysis, we chose a 1/d regime, where d is the distance in km between the grid-box and the station.

Generally, the study area shows a mean φ direction of N147° ± 13°, also confirmed by the orientation of null measurements N147°, as visible in the top rose diagrams in Figure 3. In this area, two main directional domains can be distinct, the first one located in the southeastern part characterized by an NW-SE fast direction, and the second, on the opposite side, shows an NNW-SSE general orientation.

Overall, this pattern well reflects the NE-SW active extension [Cheloni et al., 2017; D'Agostino et al., 2011], the regional stress regime [Mariucci and Montone, 2016] and the NW-SE strike of main Quaternary systems.

The anisotropy intensity, represented by the δt parameter, shows an average value of 0.061 s ± 0.009 s, while individual values range from 0.024 s to 0.230 s. In this review, we will discuss the results in terms of normalized delay

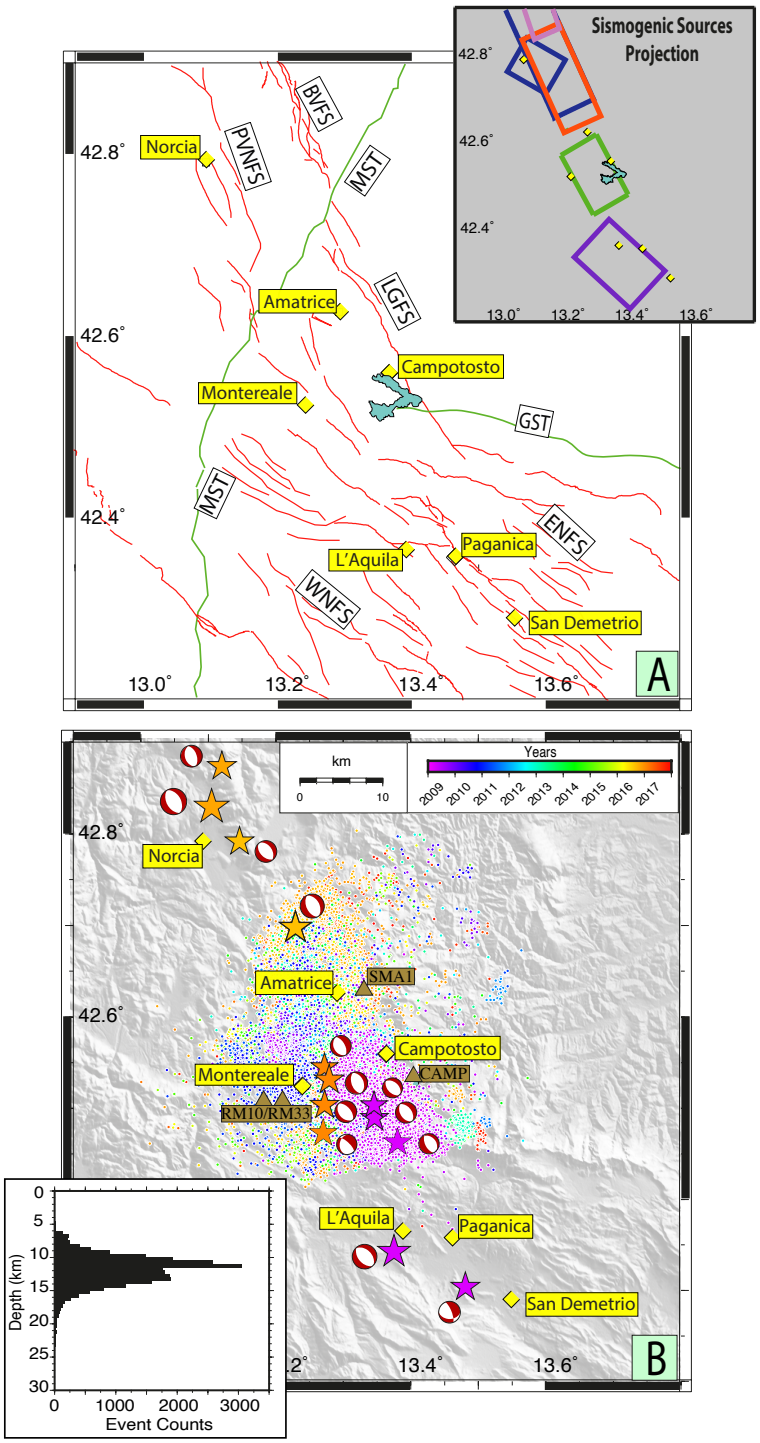

Figure 2. A) Simplified structural map of the study area, where the red and green lines represent the traces of the Quaternary active normal faults and the Neogene contractional structures, respectively. The main faults are labelled as follows: **BVFS**: Mt. Vettore – Mt. Bove Fault System; **PVNFS**: Preci-Visso-Norcia Fault System; **LGFS**: Mts della Laga – Gorzano Fault System; **ENFS**: Eastern Normal Fault System; **WNFS**: Western Normal Fault System; **MTS**: Monti Sibillini Thrust; **GTS**: Gran Sasso Thrust. In the upper right inset, the colored boxes show the seismogenic source projections of the strongest events: violet for the M_w 6.1 on 06 April 2009; orange for the M_w 6.0 on 24 August 2016; pink for the M_w 5.9 on 26 October 2016; blue for the M_w 6.5 on 30 October 2016, green for the M_w 5.5 on 18 January 2017. B) Map of the epicenters of analyzed events at the three sites (involving four stations) in the period 2009-2017, different colors represent the different years of occurrence. Stars indicate major event $M \geq 5.0$ location, and beach-balls represent their time domain moment tensor. Inset in the low left corner is the histogram of the hypocentral depth of the events. Brown triangles represent the used seismic stations, and yellow diamonds are the main villages cited in the text.

time (δtn), obtained by dividing the δt value for the hypocentral distance, because we suppose that the anisotropy strength is simply the sum of the anisotropic structures sampled by the seismic ray during its propagation in the rock volume [e.g., Crampin, 1991; Zhang et al., 2007]. Further, we use the δtn value also to compare these new results to those presented in the previous studies using the same mapping method, that is, the nearest neighbor algorithm performed by the Generic Mapping Tools [GMT 5, Wessel et al., 2013]. This method implements a simple nearest neighbor averaging operation useful to grid data when the data density is high, as in our case. The algorithm assigns an average value to each node that has one or more points within a radius centered on the node, in this study we used a grid spacing of 1 km and a searching radius of 3 km.

In Figure 3 the colored area represents those averaged and interpolated values. Single measurements of δtn range between 0.0011 s/km and 0.0236 s/km and the mean for the study area is 0.0042 ± 0.00002 s/km.

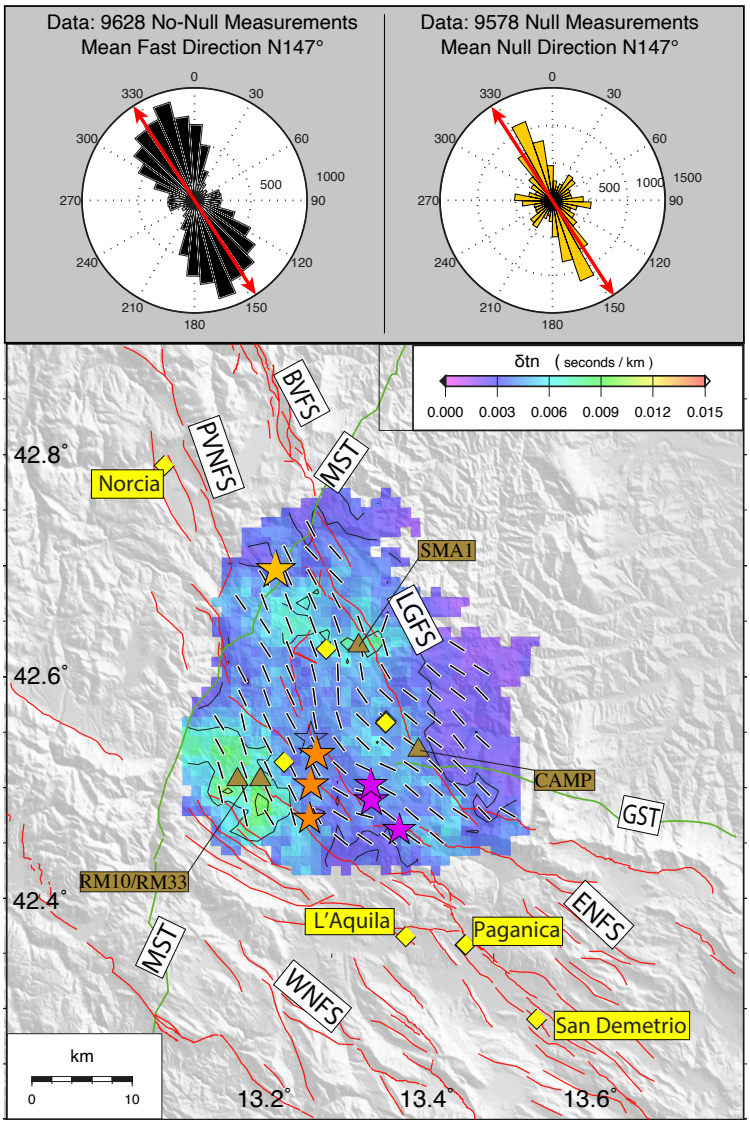

Figure 3. Map of the new splitting parameters at the three sites, involving four stations, analyzed in the time period 2009-2017. The upper plots describe the frequency distribution of fast and null measurements and the mean values for the whole area. Black bars indicate the mean φ orientations computed using TESSA; two main directional domains are recognized: 1) NW-SE on the south-eastern part, 2) NNW-SSE on the north-western side. Colored area represents the δtn spatial distribution, lower values are found nearby CAMP station which represents the footwall of the activated Quaternary Fault System while higher values characterize SMA1 area, placed between Amatrice and Montereale source and RM10/RM33 located nearby Velino aquifer with CO_2 saturated-oversaturated waters [Chiodini et al., 2020] and the intersection of 3 structural domains [Barchi et al., 2021].

Of particular interest is the location of δtn lower values found on the east side of the Monti della Laga – Gorzano Fault System, well-recorded by CAMP station. This area represents the footwall of the activated Quaternary Fault System, where minor seismicity occurred.

On the contrary, higher values of δtn (> 0.006 s/km), greater than the mean value, are found in the proximity of SMA1 and RM10/RM33 stations. SMA1 is located between the southern termination of the Amatrice source and the northern border of Montereale source, probably this area is majorly affected by the surrounding rock volume perturbations that can alter both the local stress field and crustal fracturing network. Nearby RM10/RM33 site, the biggest spatial anomaly with the highest values of δtn is located. In this area, Barchi et al. [2021] placed the intersection of 3 structural domains: Umbra-Marche, Gran Sasso and Laga, characterized by different sedimentary successions, and Chiodini et al. [2020] recognized the Velino carbonate aquifers characterized by CO_2 saturated-oversaturated waters and by the direct emissions of a CO_2-rich gas phase. These features could play an important role in diffusivity systems, such as rock permeability which, in turn, affects fluid migration.

4. Discussions

Our discussion starts with a short review of the main results of the six papers presented in the introduction, which are focused on seismic anisotropy in different areas of the Central Apennines, where we have analyzed both the background seismicity and minor earthquakes and seismic sequences.

4.1 Background seismicity and minor sequences in the Alto Tiberina Fault

The Upper Tiber River Valley hosts the Alto Tiberina Fault (ATF) low angle normal fault dipping to the east and accommodating up to 10 km of extension. Geological and seismological data show that the ATF is an active fault system that separates a seismically active hanging wall block from an aseismic footwall [Vadacca et al., 2016 and reference therein]. In the hanging wall, minor synthetic and antithetic high-angle normal faults root down into the ATF, which acts as a detachment for the SW-dipping Gubbio normal fault. The high-angle normal faults in the ATF hanging wall slip seismically, generating seismicity.

Pastori et al. [2012] analyzed the background seismicity recorded during the 2000-2001 Città di Castello passive seismic experiment [Piccinini et al., 2003] and observed a dominant NW-SE fast direction, the same orientation of the major faults. This direction is also perpendicular to the Shmin of the active extensional stress field [figure 6 in Pastori at al., 2012].

The means of φ, at the selected 13 stations, are NW-SE roughly parallel to the main geological structures, even if there are stations with rotated directions. The normalized delay times have higher values (0.01 s/km) at stations located on the ATF hanging wall and where most of the seismicity occurs. These values suggest a percentage of anisotropy A = 3% obtained by the following formula:

$$A = Vs_{mean} \times \delta tn \times 100\ per\ cent \tag{3}$$

where Vs_{mean} represents the mean shear wave velocity and is chosen in this study to be 3.3 km s^{-1}. A comparison among mean φ directions, main geological structures and minimum horizontal stress directions [Mariucci and Montone et al., 2016 and references therein] shows a general consistency.

A detailed study of seismic anisotropy, focused on the northern portion of the SW-dipping Gubbio normal fault hosted in the hanging-wall of the ATF, was done by Guerri et al. [2012] analyzing the 2010 Pietralunga seismic sequence. The great number of measurements recorded at 2 stations made possible the analysis of the spatio-temporal variations of the anisotropic parameters. The dominant φ strikes NW-SE, parallel to the orientation of the main geological structures, but it is also consistent with the horizontal maximum stress, in agreement with the EDA-APE model.

A possible connection between the temporal variations of the anisotropic parameters and the possible stress change related to the occurrence of the mainshock M = 3.8 on 15 April 2010, during the Pietralunga seismic

sequence, is observed at station ATPI [figure 3 Guerri et al., 2012] as predicted by EDA-APE model. The dominant φ strikes NW-SE and roughly NNW-SSE respectively at the two stations, according to the total results for the whole 2010 recordings. The equal-area plots show each measurement projected according to its back-azimuth and incidence angles; the seismicity migrated in space toward NW during the time. At one of the stations, a rotation in the φ with time was observed in correspondence to the occurrence of the 15 April M = 3.8 mainshock, from apenninic to anti-apenninic directions.

4.2 The 1997 Umbria-Marche seismic sequence in the area of Colfiorito, Foligno and Assisi

The Umbria-Marche seismic sequence started on 3 September 1997 with the $M_w = 4.5$ foreshock and culminated with a $M_w = 6.0$ on 26 September, followed by several aftershocks.

The shear wave splitting analysis, done by Piccinini et al. [2006], revealed a clear S-wave splitting with a prevalent φ direction of about N140° and average δt of 0.06 s [figure 3 in Piccinini et al., 2006]. φ is parallel to the strike of the major normal-fault system of the area and to the maximum horizontal stress active in the region. δt value testifies to a highly fractured crustal volume with a crack density near the critical value (10% anisotropy). The observed directions of S-wave polarization are interpreted as the alignment direction of fluid-filled fractures or cracks located in the sedimentary carbonatic coverage of the studied crustal volume, in agreement with the EDA model. To corroborate the EDA model interpretation, the authors also investigated temporal variations of anisotropic parameters. The two predominant φ, about N140° and N100°, observed in the frequency distribution of the anisotropic parameter are found at different stations in different time windows. The presence of high-pressure fluids in the investigated crust induced the authors to speculate that variations in the observed anisotropic parameters during the evolution of the sequence may be due to transient changes in the stress field and consequently in the fluid pore pressure.

4.3 The 2009 L'Aquila seismic sequence on the Paganica-San Demetrio and Campotosto faults

On 6 April 2009 (01:32 GMT), a M_w 6.3 earthquake struck L'Aquila in central Italy. The mainshock was preceded by a foreshock sequence that lasted ~6 months and was characterized by earthquakes clustering around the mainshock nucleation area. The largest foreshock ML = 4.0 occurred on 30 March. Two classes of seismological observables were investigated: Vp/Vs and SWS parameters. Variations of Vp/Vs ratio and of the anisotropic parameters during the preparatory phase of the L'Aquila earthquake have been presented in figure 3 of Lucente et al. [2010] for the station AQU, located in L'Aquila town.

These variations in the studied parameters reached paroxysmal manifestations about a week before the main shock occurrence. The prevalent carbonatic nature of the seismogenic crust in Italy makes it a favorable candidate for the formation of fluid reservoirs at depth; moreover, the deep thrusts and low-angle normal faults could act as traps (structural seal) in which fluids could accumulate and generate overpressurized reservoirs. The authors described the process of fluid diffusion that played a key role in the L'Aquila earthquake nucleation. The variation of the studied parameters during the preparatory phase of the L'Aquila earthquake demonstrates that a complex sequence of dilatancy and fluid-diffusion processes affected the rock volume surrounding the nucleation area. The time variations of anisotropic parameters can be described by EDA-APE interpretative models and are observed in the temporal series reported by Lucente et al. [2010].

Comparisons of these findings with passive image interferometry based on the cross-correlations of the ambient seismic noise have shown significant drops in the relative velocity variations accompanying the occurrence of the mainshocks [Piccinini et al., 2012].

Baccheschi et al. [2016] analyzed seismic anisotropy using thousands of earthquakes recorded during the 2009 L'Aquila seismic sequence by 55 closely spaced stations operating in the area. The authors explained the observed pattern as due to the combination of both the shear-fabric of the fault zones (SIA) and the presence of a widespread distribution of stress-aligned fluid-saturated cracks (EDA).

At some stations, fast axes deviate from NW-SE and change their orientations accordingly to the strike of the faults. In the southeastern part of the region, φ change their orientation to become orthogonal to the strike of faults and to the S_{Hmax}. Such deviations from the general trend are explained by local structural complexities related to deep buried NE-SW fault systems, or by zones bearing overpressurized fluids, which are responsible for the 90° flips

of fast axes and the generation of trapped waves. δt does not show any variations in depth, supporting the hypothesis that most of the anisotropy is confined in the uppermost crust. Notably, on an averaged map, lower δt correspond to the regions of the main shock fault plane [black box with red contours in figure 8 in Baccheschi et al., 2016] where large slip occurred, whereas lower values are confined to the edges of the rupture patches: high values of coseismic slip (>0.7 m) are associated with low values of δt (<0.06 s).

4.4 The 2016-2017 seismic sequence at Amatrice-Visso-Norcia

In 2016-2017, Central Italy was struck by the strongest Italian seismic sequence since 1980. On August 24th 2016 a M_w 6.0 mainshock occurred close to the villages of Accumoli and Amatrice. It was followed, on 26 October 2016, by two M_w 5.6 and M_w 5.9 earthquakes close to Visso village to the north; on October 30th 2016 the largest earthquake of the sequence struck near Norcia (M_w 6.5), reactivating the entire length of the fault system. The sequence continued on 18 January 2017 with four $M_w \geq 5.0$ earthquakes which occurred to the south toward L'Aquila town.

Pastori et al. [2019] presented a large shear wave splitting high-quality data collection for the Central Apennines. The 11865 φ-δt couples show great variability in space and time and highlight the structural complexity of the study region. The mean φ strikes N146°, but locally different patterns are recognized. To evidence this spatial variability, the area was divided into 6 sectors [figure 7 in Pastori et al., 2019] having the following characteristics: sectors 1-2, located in the NW, have a NW-SE φ; sector 3, in the North, shows the major variability, with direction varying from NE-SW to E-W and NW-SE; sector 4, in the southern part, shows a φ direction between N-S and WNW-ESE; sector 5, in the South-East, has a NE-SW φ direction and finally sector 6, in the southeastern, shows an E-W φ direction.

We believe that the presence of seismic anisotropy is caused by the active stress, responsible for the presence of pervasive fluid-filled stress-aligned crack systems (EDA-APE models) in sector 3. In the other sectors, anisotropy seems to be influenced by both stress and structural complexity (EDA and SIA models). We cannot discern between models in the extensional regime due to the coincidence of the S_{Hmax} direction and the strike of major faults.

The mean δt for the area is 0.064 ± 0.030 s, with single values in the range of 0.024 s - 0.290 s; δtn distribution in space [figure 10 of Pastori et al., 2019] helped us to define the most fractured rock volumes in the crustal region interested in the Amatrice-Visso-Norcia seismic sequence.

The different lithologies present in the study area probably played a role in determining the intensity of seismic anisotropy at shallow depths, with high value characterizing the carbonate rocks with respect to the turbiditic deposits. The higher values of δtn (> 0.007 s/km) are located on the western side of the activated fault systems, while the eastern part is characterized by the presence of lower δtn values (< 0.005 s/km). The rocks on the western side of the major seismogenic faults activated during the seismic sequence are heavily stressed and, in some patches, especially at the edges and at the intersections between faults, probably contain fluids channeled, trapped and over-pressurized.

The datasets analyzed in the six papers briefly resumed above, are presented in Figure 4 both as event locations and as rose diagrams plotted on each station; moreover, individual measurements have been also collected in a single Excel file available as Table A1.

In the northern area, the fewest events were analyzed producing fewer results, in terms of shear wave splitting measurements, with respect to the southern sequences.

As visible in Figure 4, the different studies analyzed seismicity in different regions in the Central Apennines and between the Gubbio – ATF portion and the seismic sequences of Umbria-Marche, L'Aquila, Amatrice-Visso-Norcia a significant gap is present. The observed spatial variability in φ directions is more pronounced in the Gubbio-ATF area, probably related to few results. Taking into account the number of results and their spatio-temporal continuity in the different regions, we decided to represent in a single figure only the measurements of the southern portion containing the L'Aquila and Amatrice-Visso-Norcia major seismic sequences.

Looking at the overall distribution of the splitting results recorded at 86 seismic stations, presented in Figure 5 as interpolated values of φ and δtn, we observe a more intense anisotropy strength (>0.006 s/km) near the strongest events (M > 5), all concentrated in the hanging-wall of the activated fault systems. In this area also occurred the majority of earthquakes that, in some cases, promoted the crack opening and fluid recall along preferential pathways generated by microcrack coalescence, and in others especially where fault intersections are present, fluids could be trapped and, under some stress conditions, reach the overpressure state. In general, the delay time values found in

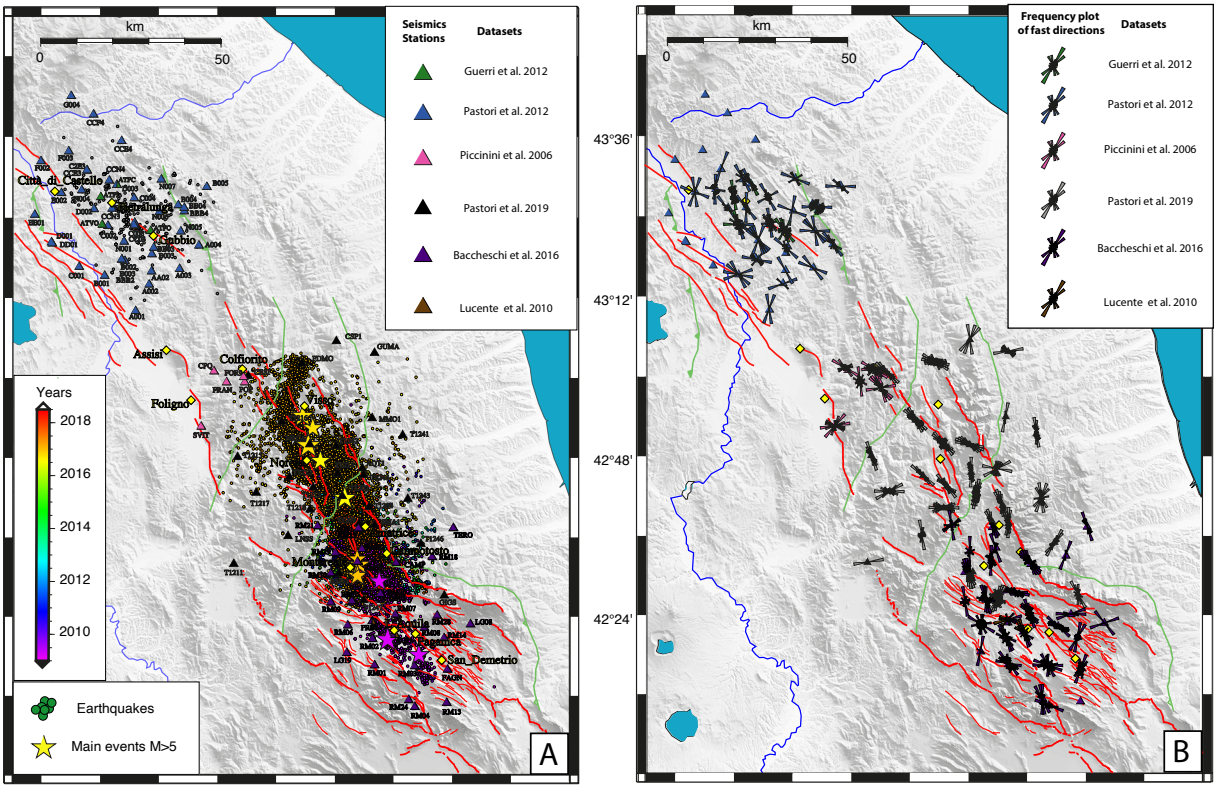

Figure 4. A) Map of events (circles) and stations (triangles) analyzed to study shear wave splitting and presented in this paper. Yellow diamonds represent the cited villages in the main text. Stars are the strongest events ($M_w > 5$) colored according to the occurrence time. B) Map of the 106 analyzed stations with frequency plot of fast directions measured. The colors of the stations indicate the different datasets, as well as the associated rose diagrams. For four sites (ATVO/COO2, ATPC/D003, RM10/RM33 and RM25/T1299/LG01) the associate rose diagrams are bicolor, in this case, the stations belong to a different dataset (see legend).

the footwall of the fault system are lower, pointing to the presence of stronger anisotropy in the hanging wall than in the footwall of the studied fault system.

To compare the anisotropic results, we also superimposed the mean φ directions, obtained by TESSA [Johnson et al., 2011], on the interpolated map of the δtn. The fast directions show two dominant average orientations: in the central part, the NNW-SSE trend prevails, while the NW-SE trend persists in the northwest and southeast areas. Furthermore, some deviations are noted, which could be related to the local reorganization of the microcracks, in turn, due to stress and fracture field variations, fluid migrations and pore pressure changes.

The general trend agrees with both the direction of the extensional quaternary and inherited compressive fault systems, focal mechanisms and local extension regime, as predicted by both EDA [Crampin, 1993] and SIA [Zinke and Zoback, 2000] interpretative models. Unfortunately, in a region where the S_{Hmax} direction and the major fault strike coincide, it is difficult to discriminate between the prevailing sources of anisotropy.

With the aim to discern between prevailing sources of anisotropy, we needed to study the spatio-temporal changes of anisotropic parameters in a sector with good data covering. This zone is represented by the overlapped area for which we recovered and analyzed the data at 3 sites (see section 3) to fill the temporal gap between the L'Aquila and Amatrice sequences (yellow dashed box in Figure 5). This area is very interesting for many reasons: i) it is located at the intersection of three different structural domains: Umbra-Marche, Gran Sasso and Laga [Barchi et al., 2021], characterized by different sedimentary successions that could affect fluid migrations and microcracks opening or closing; ii) it is in between of two large carbonate aquifers: the Gran Sasso on the east and the Velino on the west [Chiodini et al., 2020], the latter characterized by CO_2 saturated-oversaturated waters and by the direct emissions of a CO_2-rich gas phase; iii) the last strongest events ($M \leq 5.5$) for both sequences converged in this area, and iiii) the CFTI5Med and CPTI15 catalogues [Guidoboni et al., 2019; Rovida et al., 2022] report a strong historical earthquake Mw 6.67 in 1703, but during the last sequences, the maximum recorded magnitude is 5.5.

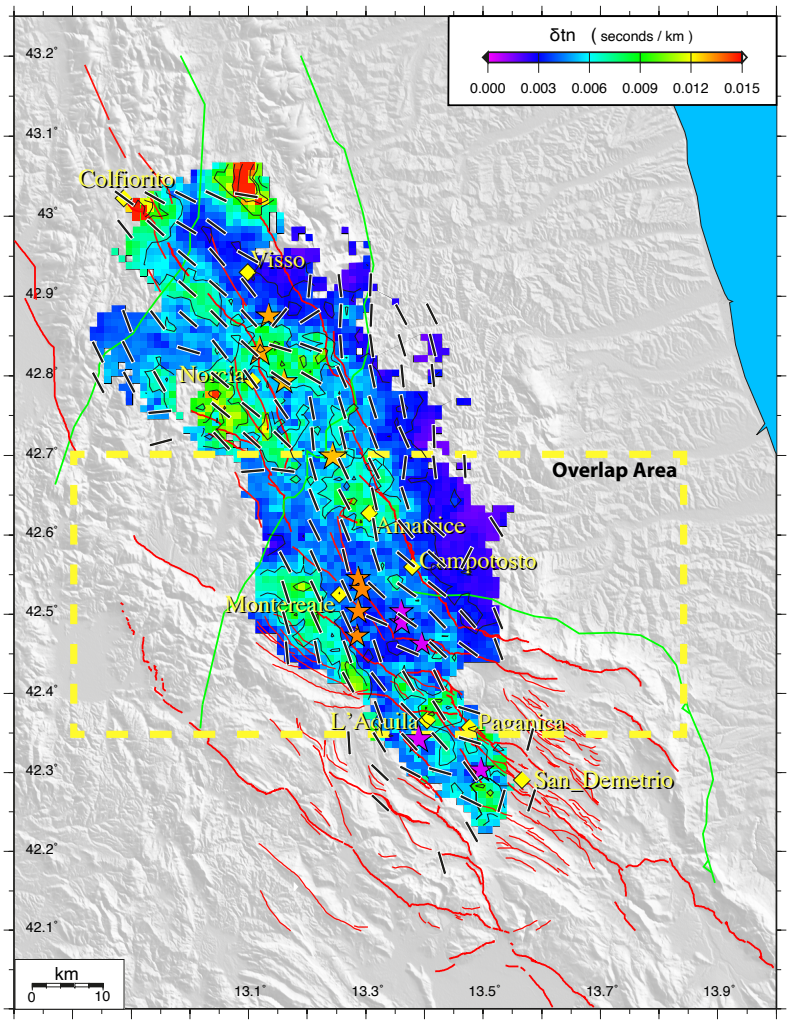

Figure 5. Integrated map of anisotropic parameters recorded during the L'Aquila and Amatrice-Visso-Norcia major seismic sequences at 86 seismic stations. Colored area represents the normalized delay time values interpolated using the GMT nearest neighbor algorithm; the green-yellow-red areas indicate the highest δtn values (>0.006 s/km) greater than the mean value 0.0042 s/km. Black bars are the mean fast polarization directions for those grid boxes having standard error and standard deviation of less than 10° and 30°, respectively. Stars indicate the events with M>5 and their color represent the occurrence time (see the scale in Fig. 8). The yellow dashed box indicates the area analyzed in Figure 6.

We selected and analyzed 3 time periods (Figure 6) and all data was recorded inside the yellow dashed box in Figure 5. During period 1, from 01/01/2009 to 31/12/2010 which includes the L'Aquila sequence, higher values of δtn (> 0.06 s/km) illuminated two main zones: 1) the northern termination of the L'Aquila source, where mixed-up φ directions vary from NNW-SSE to NW-SE and 2) the western external area of the Montereale source, where fast directions rotate from NW-SE to N-S orientation.

In period 2, from 01/01/2011 to 31/12/2015 in which strong events are not reported, we found an increased size and value of δtn (up to 0.012 s/km) of the anomaly found in period 1 in the western area of Montereale, in this case, a stable NNW-SSE φ orientation is visible. Furthermore, a slight grown-up of δtn is also registered at the southern edge of the Amatrice source nearby, where 8 months later, the M 6.1 Amatrice mainshock occurred.

In period 3, from 01/01/2016 to 31/12/2017 which includes the Amatrice sequence, both previous δtn anomalies increased their values (up to 0.013-0.014 s/km on the western side) and size, moreover, another small peak (>0.06 s/km) is also recognized in the central-eastern part of the Montereale source. In correspondence to these anomalies, the φ is stable and coherent to the general geo-structural context. Instead, the great discrepancy in the NW-SE or NNW-SSE general trend of φ measurements is visible in the northwestern area, assuming an E-W orientation, and on the east side where an anti-apenninic direction is reported.

The anisotropic pattern described by shear wave splitting well delineates the complexity of tectonic structures and transient stress variations, and also analyzing this long-term data the ambiguity on the prevalent anisotropic source remains.

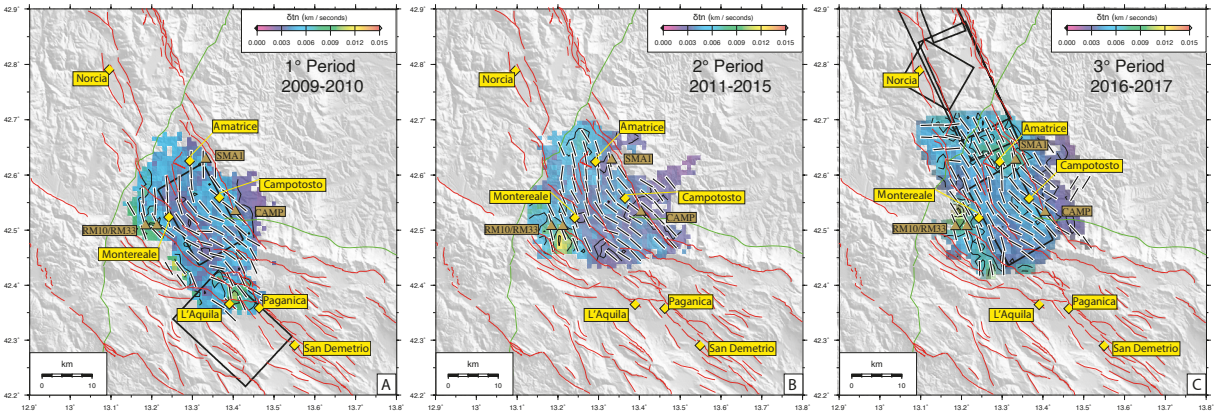

Figure 6. Spatio-temporal evolution of the new dataset, falling back to the yellow dashed box in Figure 5, and recorded at the three sites: SMA1, CAMP, RM10/RM33 during the period 2009-2017. The anisotropic pattern was divided into three different time periods: A) from 01/01/2009 to 31/12/2010 which includes the L'Aquila sequence; B) from 01/01/2011 to 31/12/2015 in which no strong events are reported; C) from 01/01/2016 to 31/12/2017 which includes the Amatrice sequence. In each map, the activated seismogenic sources (black boxes) are plotted. See the text for details on the interpretations.

5. Conclusions

In this review, we made available all the anisotropic datasets analyzed in the last two decades and presented in the six papers briefly resumed in section 2, covering about 160 km from north to south along the Central Apennines.

In general, the fast directions in the studied area show two dominant average orientations: NNW-SSE and NW-SE, in agreement with the articulated fault system present in this sector of Apenninic chain. Some deviations are noted, which could be related to the local reorganization of the microcracks, in turn, due to stress and fracture field variations, fluid migrations and pore pressure changes.

The general trend agrees with both the direction of the extensional quaternary and inherited compressive fault systems, focal mechanisms and local extension stress field. In this context, where the S_{Hmax} direction and the major fault strike coincide, it is difficult to discriminate if the prevailing source of anisotropy is related to the active stress or to the inherited fracture field. In figure 7 we report a summary of the different mechanisms that we believe to be responsible for the shear wave splitting in the crust, according to the main interpretative models described in the 1.2 paragraph. The observation of changes in time of the anisotropic parameters, found by the authors of the 6 papers reviewed and by the new results, points to the presence of EDA-APE mechanisms, where a more intensity of anisotropy is recorded. These areas are found especially at the edges and at the intersections between faults, probably containing fluids channelled, trapped, and/or over pressurized, in this condition the local stress can change causing a reorientation of micro cracks, recorded by a flip in the fast axes. In the other sectors, anisotropy seems to be influenced by both stress and structural complexity, EDA and SIA mechanisms, respectively.

Instead, the SIA mechanism is recognized, where fast polarization directions seem to be controlled by the orientation of the Monti Sibillini Thrust. The influence of this major thrust is found mainly to the east of the superficial trace of the Monti Sibillini Thrust up to a distance of about 10 km (Figure7); a similar distance of influence on anisotropic parameters by major a fault was also observed in the Tibetan plateau [Shi et al., 2020].

The lower values of delay time are found in the footwall of the analyzed fault systems activated during the seismic crises; this result point to the presence of stronger anisotropy in the hanging wall more than in the footwall of the studied fault systems.

Studying the spatio-temporal changes of anisotropic parameters in a sector with a good data covering, if we consider also long time periods, we could not exclude either stress or structural contribution to the crustal seismic

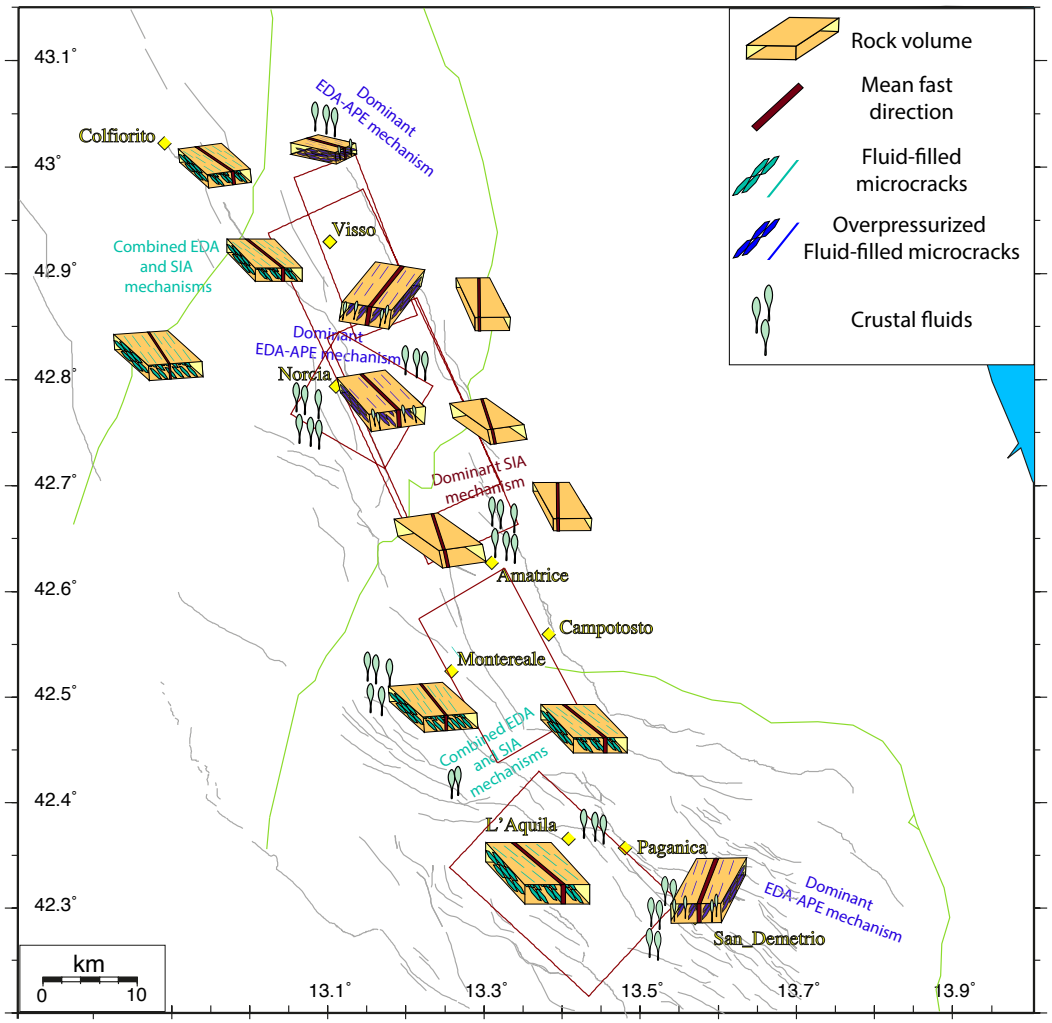

Figure 7. Schematic summary of main mechanisms generating crustal shear-wave splitting.

anisotropy recovered in the Central Apennines region, therefore both EDA [Crampin, 1993] and SIA [Zinke and Zoback, 2000] models can be considered plausible interpretations.

Acknowledgements. The authors are grateful to all operators who installed and serviced the temporary seismic stations managed by INGV. We would like to follow up by thanking all the INGV staff on shifts in the surveillance room in Rome for their work and the Bollettino Sismico Italiano working group (http://terremoti.ingv.it/bsi) for making available the files of the manually revised P- and S-phase pickings.
Finally, we are grateful to the Guest Editor George Kaviris and the two anonymous reviewers for their thorough reviews that improved the final version of the manuscript.

Data e sharing resources. The pickings and waveform data of earthquakes used for the splitting analysis are respectively available at ISIDe (ISIDe working group (2016) version 1.0, DOI: 10.13127/ISIDe) and at EIDA (European Integrated Data Archive http://eida.rm.ingv.it/).
The data of used stations are from the Italian National Seismic Network (doi.org/10.13127/SD/X0FXnH7QfY).
We used Anisomat+ [Piccinini et al., 2013] to retrieve anisotropic parameters. Fast polarization directions are plotted by means TESSA [Johnson, et al., 2011].
We used the Generic Mapping Tool [https://www.generic-mapping-tools.org/; Wessel and Smith, 2013] to prepare some figures, plots and to interpolate delay time values.
All figures were edited with Adobe Illustrator CS6 (adobe.com/it/products/illustrator.html).

Appendices

A.1 Table containing the anisotropic database, recovered by the review of previous papers and the new dataset along the Central Apennines. In each sheet the results, of each individual paper, are reported.

A.2 Table containing the station coordinates used in this work.

References

Amato A., R. Azzara, C. Chiarabba, G.B. Cimini, M. Cocco, M. Di Bona, L. Margheriti, S. Mazza, F. Mele, G. Selvaggi, A. Basili, E. Boschi, F. Courboulex, A. Deschamps, S. Gaffet, G. Bittarelli, L. Chiaraluce, D. Piccinini, M. Ripepe (1998). The 1997 Umbria-Marche, Italy, Earthquake Sequence: A first look at the main shocks and aftershocks (1998), Geophys. Res. Lett., 2861-2864, 25, 15, 0094-8276. https://doi.org/10.1029/98GL51842.

Baccheschi P., M. Pastori, D. Piccinini D., L. Margheriti (2016). Shear wave splitting of the 2009 L'Aquila seismic sequence: fluid saturated microcracks and crustal fractures in the Abruzzi region (Central Apennines, Italy). Geophys. J. Int., 204, 1531-1549, doi: 10.1093/gji/ggv536.

Balfour, N.J., Cassidy, J.F. and S.E. Dosso, (2012). Crustal anisotropy in the forearc of the Northern Cascadia Subduction Zone, British Columbia, Geophys. J. Int., 188, 165-176.

Barchi M.R., F. Carboni, M. Michele, M. Ercoli, C. Giorgetti, M. Porreca, S. Azzaro, L. Chiaraluce, The influence of subsurface geology on the distribution of earthquakes during the 2016-2017 Central Italy seismic sequence, Tectonophysics, Volume 807, 2021, 228797, ISSN 0040-1951, https://doi.org/10.1016/j.tecto.2021.228797.

Boness, N. L., & Zoback, M. D. (2006). Mapping stress and structurally controlled crustal shear velocity anisotropy in California. Geology, 34(10), 825-828. https://doi.org/10.1130/G22309.1.

Boness, N.L. & Zoback, M.D., 2004. Stress-induced seismic velocity anisotropy and physical properties in the SAFOD pilot hole in Parkfield, CA, Geophys. Res. Lett., 31, L15S17, doi:10.1029/2003GL019020.

Bouin, M.P., Te´llez, J. & Bernard, P., 1996. Seismic anisotropy around the Gulf of Corinth, Grrece, deduced from the three-component seismograms of local earthquakes and its relationship with crustal strain, J. geophys. Res., 101, 5797-5811.

Bowman, J. R., & Ando, M. (1987). Shear-wave splitting in the upper-mantle wedge above the Tonga subduction zone. Geophysical Journal of the Royal Astronomical Society, 88(1), 25-41. https://doi.org/10.1111/j.1365-246X.1987.tb01367.x.

Buontempo, L. & Wuestefeld, A., 2013. Complex fault structure interactions of crustal shear zones revealed by seismic anisotropy: an example in the eastern betic cordillera (Spain), TerraNova, 25, 57-64.

Cheloni, D., de Novellis, V., Albano, M., Antonioli, A., Anzidei, M., Atzori, S., et al. (2017). Geodetic model of the 2016 Central Italy earthquake sequence inferred from InSAR and GPS data. Geophysical Research Letters, 44, 6778-6787. https://doi.org/10.1002/ 2017GL073580.

Chiarabba, C., et al. (2009), The 2009 L'Aquila (central Italy) MW6.3 earthquake: Main shock and aftershocks, Geophys. Res. Lett., 36, L18308, doi:10.1029/2009GL039627.

Chiodini G., C. Cardellini, F. Di Luccio, J. Selva, F. Frondini, S. Caliro, A. Rosiello, G. Beddini, G. Ventura. Correlation between tectonic CO2 Earth degassing and seismicity is revealed by a 10-year record in the Apennines, Italy. Sci. Adv., 6 (35) (2020), Article eabc2938, 10.1126/sciadv.abc2938.

Cirella, C., Piatanesi, A., Tinti, E., Chini, M. & Cocco, M., 2012. Com- plexity of the rupture process during the 2009 L'Aquila, Italy, earthquake, Geophys. J. Int., 190, 607-621.

Cochran, E.S., Li, Y.-G. & Vidale, J.E., 2006. Anisotropy in the shallow crust observed around the San Andreas fault before and after the 2004 M 6.0 Parkfield earthquake, Bull. seism. Soc. Am., 96, S364-S375.

Crampin, S. (1991). Wave propagation through fluid-filled inclusions of various shapes: Interpretation of extensive-dilatancy anisotropy. Geophysical Journal International, 107, 611-623.

Crampin, S. (1993). Arguments for EDA. Can. J. Explor. Geophys. 29, 18-30.

D'Agostino, N., Mantenuto, S., D'Anastasio, E., Giuliani, R., Mattone, M., Calcaterra, S., et al. (2011). Evidence for localized active extension in the central Apennines (Italy) from global positioning system observations. Geology, 39(4), 291-294. https://doi.org/10.1130/ G31796.1.

Eken, T., Bohnhoff, M., Bulut, F., Can, B. & Aktar, M., 2013. Crustal anisotropy in the Eastern Sea of Marmara Region in Northwestern Turkey, Bull. seism. Soc. Am., 103(2A), 911-924.

Evans R., Effects of the free surface on shear wavetrains, Geophys. J. Int., 76, 1, 165-172.

Gao, Y. & Crampin, S., 2008. Shear-wave splitting and Earthquake forecasting, TerraNova, 20(6), 440-448.

Gao, Y., Wang, P.-D., Zheng, S.-H., Wang, M., Chen, Y.-T. & Zhou, H.-L., 1998. Temporal changes in shear-wave splitting at an isolated swarm of small earthquakes in 1992 near Dongfang, Hainan Island, southern China, Geophys. J. Int., 135, 102-112.

Gao, Y., Wu, J., Fukao, Y., Shi, Y. & Zhu, A., 2011. Shear wave splitting in the crust in North China: stress, faults and tectonic implications, Geophys. J. Int., 187, 642-654.

Guerri M., Pastori M., Margheriti L., D'Alema E., Piccinini D., Barchi M.R. Seismic anisotropy and micro-seismicity in the upper crust at north of Gubbio Basin (Central Italy): relation with the subsurface geological structures and the active stress field. 31° Convegno GNGTS – Gruppo Nazionale di Geofisica della Terra Solida, TEMA 1: Geodinamica, Sessione 1.1: Terremoti e Faglie, pag. 134-143.Potenza 20-22 Novembre 2012.

Guidoboni E., Ferrari G., Tarabusi G., Sgattoni G., Comastri A., Mariotti D., Ciuccarelli C., Bianchi M.G., Valensise G. (2019), CFTI5Med, the new release of the catalogue of strong earthquakes in Italy and in the Mediterranean area, Scientific Data 6, Article number: 80 (2019). doi: https://doi.org/10.1038/s41597-019-0091-9.

Hiramatsu, Y., Iwatsuki, K., Ueyama, S. & Iidaka, T. & Japanese University Group, 2010. Spatial variation in shear wave splitting of the upper crust in the zone of inland high strain rate, central Japan, Earth Planets Space, 62, 675-684.

Hurd, O. & Bohnhoff, M., 2012. Stress- and Structure-Induced shear-wave anisotropy along the 1999 Izmit Rupture, Northwest Turkey, Bull. seism. Soc. Am., 102(5), 2177-2188.

Improta, L., Latorre, D., Margheriti, L. et al. Multi-segment rupture of the 2016 Amatrice-Visso-Norcia seismic sequence (central Italy) constrained by the first high-quality catalog of Early Aftershocks. Sci Rep 9, 6921 (2019). https://doi.org/10.1038/s41598-019-43393-2.

Johnson, J. H., Savage, M. K., & Townend, J. (2011). Distinguishing between stress-induced and structural anisotropy at mount ruapehu volcano, New Zealand. Journal of Geophysical Research, 116, B12303. https://doi.org/10.1029/2011JB008308.

Kapetanidis, V.; Michas, G.; Kaviris, G.; Vallianatos, F. Spatiotemporal Properties of Seismicity and Variations of Shear-Wave Splitting Parameters in the Western Gulf of Corinth (Greece). Appl. Sci. 2021, 11, 6573. https://doi.org/10.3390/app11146573.

Li, Z., Zhang, H. & Peng, Z., 2014. Structure-controlled seismic anisotropy along the Karadere-Düzce branch of the North Anatolian Fault revealed by shear-wave splitting tomography, Earth planet. Sci. Lett., 391, 319-326.

Liu, Y., Crampin, S. & Main, I., 1997. Shear-wave anisotropy: spatial and temporal variations in time delays at Parkfield, central California, Geo- phys. J. Int., 130, 771-785.

Liu, Y., Zhang, H., Thurber, C. & Roecker, S., 2008. Shear wave anisotropy in the crust around the San Andreas fault near Parkfield: spatial and temporal analysis, Geophys. J. Int., 172, 957-970.

Lucente F.P., De Gori P., Margheriti L., Piccinini D., Di Bona M., Chiarabba C. and Piana Agostinetti N.; 2010: Temporal variation of seismic velocity and anisotropy before the 2009 M_w 6.3 l'Aquila earthquake, Italy. (2010) Geology, 38, 1015-1018.

Mariucci MT, Montone P. Contemporary stress field in the area of the 2016 Amatrice seismic sequence (central Italy). Ann. Geophys. 2016 Nov. 17. Available from: https://www.annalsofgeophysics.eu/index.php/annals/article/view/7235.

Martin, P., Arroucau, P. & Vlahovic, G., 2014. Shear-wave splitting study of crustal anisotropy in the New Madrid Seismic Zone, Bull. seism. Soc. Am., 194(3), 1100-1110.

Matharu, G., Bostock, M.G., Christensen, N.I. & Tromp, J., 2014. Crustal anisotropy in a subduction zone forearc: Northern Cascadia, J. geophys. Res., 119, 7058-7078.

Padhy, S. & Crampin, S., 2006. High pore-fluid pressures at Bhuj, inferred from 900-flips in shear-wave polarizations, Geophys. J. Int., 164, 370- 376.

Pastori M., Baccheschi P., Margheriti L. – Shear wave splitting evidence and relations with stress field and main fault from the "Amatrice-Visso-Norcia seismic sequence". (2019) Tectonics, 38. https://doi.org/10.1029/2018TC005478.

Pastori M., Piccinini D, Valoroso L., Wuestefeld A., Zaccarelli L., Bianco F., Kendall M., Di Bucci D., Margheriti L. and Barchi M.R. – Crustal fracturing field and presence of fluid as revealed by seismic anisotropy: case histories from seismogenic areas in the Apennines (Italy). Bollettino di Geofisica Teorica e Applicata, 2012, Vol. 53 Vol. 53, n.4, December 2012 pp. 417-433. DOI 10.4430/bgta0047.

Piccinini D., Margheriti M., Chiaraluce L. and Cocco M.; 2006: Space and time variation of crustal anisotropy during the 1997 Umbria-Marche, Central Italy, seismic sequence. Geophys. J. Int., 167, 1482-1490.

Piccinini D., Pastori M., Margheriti L. – ANISOMAT+: an automatic tool to retrieve seismic anisotropy from local earthquakes. Computers & Geosciences, Volume 56, July 2013, Pages 62-68, ISSN 0098-3004, DOI:10.1016/j.cageo.2013.01.012.

Piccinini D., Zaccarelli L., Pastori M., Margheriti L., Lucente F.P., De Gori P., Faenza L. and G. Soldati; 2012 Spatio-temporal monitoring of seismic wave velocities in the upper crust gngts extended abstract.

Piccinini, Marco Cattaneo, Claudio Chiarabba, Lauro Chiaraluce, Martina De Martin, Massimo Di Bona, Milena Moretti, Giulio Selvaggi, Paolo Augliera, Daniele Spallarossa, Gabriele Ferretti, Alberto Michelini, Aladino Govoni, Paolo Di Bartolomeo, Marco Romanelli and Julius Fabbri (2003). A microseismic study in a low seismicity area of Italy: the Città di Castello 2000-2001 experiment. Annals of Geophysics, VOL. 46, N. 6, December 2003.

Rovida A., Locati M., Camassi R., Lolli B., Gasperini P., Antonucci A. (eds), 2022. Italian Parametric Earthquake Catalogue (CPTI15), version 4.0. Istituto Nazionale di Geofisica e Vulcanologia (INGV). https://doi.org/10.13127/CPTI/CPTI15.4.

Savage, M. K. (1999), Seismic anisotropy and mantle deformation: What have we learned from shear wave splitting?, Rev. Geophys., 37(1), 65-106, doi:10.1029/98RG02075.

Schutt, D., Humphreys, E. & Dueker, K. Anisotropy of the Yellowstone Hot Spot Wake, Eastern Snake River Plain, Idaho. Pure appl. geophys. 151, 443-462 (1998). https://doi.org/10.1007/s000240050122.

Shi Y., Yuan Gao, Xu-zhang Shen, Kelly H. Liu, (2020) Multiscale spatial distribution of crustal seismic anisotropy beneath the northeastern margin of the Tibetan plateau and tectonic implications of the Haiyuan fault, Tectonophysics, Vol. 774, 2020, 228274 ISSN 0040-1951, https://doi.org/10.1016/j.tecto.2019.228274.

Syracuse, E. et al., 2012. Temporal and spatial evolution of hypocenters and anisotropy from the Darfield aftershock sequence: implications for fault geometry and age, N.Z. J. geol. Geophys., 55, 287-293.

Vadacca, Luigi & Casarotti, Emanuele & Chiaraluce, Lauro & Cocco, Massimo. (2016). On the mechanical behaviour of a low-angle normal fault: The Alto Tiberina fault (Northern Apennines, Italy) system case study. Solid Earth. 7. 1537-1549. 10.5194/se-7-1537-2016.

Verdon J.P., Doug A. Angus, J. Michael Kendall, and Stephen A. Hall. The effect of microstructure and nonlinear stress on anisotropic seismic velocities. Geophysics 2008 73:4, D41-D51.

Vinnik, L., and R. Kind (1993) Ellipticity of teleseismic S-particle motion, Geophys. J. Int., 113, 165-174, 1993.

Wessel, P., W. H. F. Smith, R. Scharroo, J. Luis, and F. Wobbe, Generic Mapping Tools: Improved Version Released, EOS Trans. AGU, 94(45), p. 409-410, 2013. doi:10.1002/2013EO450001.

Zatsepin, S. V., & Crampin, S. (1997). Modelling the compliance of crustal rock—I. Response of shear-wave splitting to differential stress. Geophysical Journal International, 129, 477-494.

Zhang, H. J., Liu, Y. F., Thurber, C., & Roecker, S. (2007). Three-dimensional shear-wave splitting tomography in the Parkfield, California region. Geophysical Research Letters, 34, L24308. https://doi.org/10.1029/2007GL031951.

Zhang, Z. & Schwartz, S.Y., 1994. Seismic anisotropy in the shallow crust of the Loma Prieta segment of the San Andreas fault system, J. Geophys. Res., 99, 9651-9661.

Zinke, J.C. & Zoback, M.D., 2000. Structure-related and stress-induced shear-wave velocity anisotropy: observations from microearthquakes near the Calaveras fault in central California, Bull. seism. Soc. Am., 90, 1305-1312.

***CORRESPONDING AUTHOR: Marina PASTORI**,
Istituto Nazionale di Geofisica e Vulcanologia, Osservatorio Nazionale Terremoti, Roma, Italy
e-mail: marina.pastori@ingv.it